SANISAND-MS-T: Simple ANIsotropic SAND model with Memory Surface for Temperature effects

Yize Pan¹ and Alessandro F. Rotta Loria^{1*}

⁴ Subsurface Opportunities and Innovations Laboratory, SOIL, Department of Civil and Environmental Engineering,

Northwestern University, 2145 Sheridan Road, Evanston, Illinois 60208, USA

*Corresponding author: af-rottaloria@northwestern.edu

Abstract

In recent years, growing investigations have explored the temperature effects on the mechanics of sands, unveiling notable deformations caused by individual and multiple thermal cycles. Despite these advances, the simulation of temperature effects on the mechanics of sands resorts to limited constitutive models – none of which can suitably capture thermal cycling effects. This study aims to advance the state-of-the-art by exploring the potential of extending the SANISAND-MS model into a SANISAND-MS-T model that can capture thermal cycling effects in sands via a thermo-mechanical coupling. The paper assesses the model capabilities by using a single set of parameters to simulate the deformation of 1 Q-ROK silica sand subjected to monotonic mechanical loading under triaxial conditions, mechanical loading and unloading under oedometric conditions. The results demonstrate the capabilities of SANISAND-MS-T model to simulate the evolution of sand deformation subjected to thermal cycling. In addition, the results explore the role of thermal cycling effects in achieving a terminal density for sands. This work offers new insights into long-term sand deformation and a new tool to simulate the ultimate deformation in granular materials subjected to thermal cycles for

Keywords: constitutive modeling; sands; granular materials; thermal cycling; deformation,

1. Introduction

scientific and engineering purposes.

- 26 Sands and other granular materials continuously undergo temperature variations. These temperature
- 27 variations can be applied from hundreds to million times to sands surrounding technologies utilized for
- 28 geothermal energy harvesting (Yavari et al. 2014, Ng et al. 2016a, Wang et al. 2017, Laloui and Rotta Loria
- 29 2019, Kong et al. 2021, Zhao et al. 2022b), oil extraction (Zoback 2010), thermal energy storage (Lee 2013,

- 30 Chen et al. 2006, Vargas and McCarthy 2007a, Manbeck 1984, Percier et al. 2013, Zhao et al. 2016, Sassine
- et al. 2018, Mitterlehner et al. 2020), and material storage (Carson 2001, Chen et al. 2006, Dogangun et al.
- 32 2009).

- 33 Temperature variations induce deformations in sands, as shown in various experimental investigations
- 34 (Agar 1984, Agar et al. 1986, He et al. 2021, Kosar 1983, Liu et al. 2018, 2020, Ng et al. 2016b,
- 35 Sittidumrong et al. 2019, Pan et al. 2020, 2022, 2024a, 2024b) and computational studies (Sassine et al.
- 2018, Vargas and McCarthy 2007b, Dreissigacker et al. 2010, Zhou et al. 2017, Iliev et al. 2019, Zhao et
- al. 2020, Coulibaly et al. 2020, Zhao et al. 2022a, Coulibaly and Rotta Loria 2022). Recent evidence
- supports that these materials volumetrically expand upon heating and contract upon cooling (Liu et al. 2018,
- Pan et al. 2020, 2022). Upon completing a single thermal cycle, sands undergo an irreversible (plastic)
- 40 contractive deformations, even when minimal temperature variations are applied to such materials (Pan et
- al. 2020, 2022, Coulibaly and Rotta Loria 2022). This evidence involves that sands undergo cumulative
- 42 irreversible deformations upon multiple thermal cycles (under constant applied stress) (Sassine et al. 2018,
- Vargas and McCarthy 2007b, Dreissigacker et al. 2010, Iliev et al. 2019, Zhao et al. 2020, Coulibaly et al.
- 44 2020, Zhao et al. 2022a, Pan et al. 2024a, 2024b). Thermal cycling effects resemble mechanical cycling
- effects in sands (Chong and Santamarina 2016, Park and Santamarina 2019) because in both cases plastic
- 46 deformations accumulate following the cyclic application of thermal and mechanical loads, respectively,
- 47 stabilizing after a large number of loading-unloading cycles.
- 48 Despite the increasing number of studies on the thermally induced deformation of sands, only a handful of
 - constitutive models are available to capture temperature effects on the mechanics of such materials (Zhou
- et al. 2017, Coulibaly and Rotta Loria 2022, Zhao et al. 2022a) and none of them is suited to simulate
- 51 thermal cycling effects. The limited availability of constitutive models for capturing the mechanics of sands
- subjected to thermal cycling can be attributed in part to the contradictory experimental findings regarding
- 53 the influence of individual heating-cooling cycles until recent years, and partly to the lack of experimental
- evidence about the impact of multiple heating-cooling cycles on the response of such materials (Rotta Loria
- and Coulibaly 2021). However, recent studies have provided substantial experimental evidence allowing to
- 56 clarify and quantify the effects of monotonic and cyclic temperature variations on the mechanics of sands
- 57 (Pan et al. 2022, 2024a), representing useful reference for the formulation of advanced constitutive models.
- 58 Among the various constitutive models available to simulate the mechanics of sands, the SANISAND
- 59 model family (Dafalias and Manzari 2004, Taiebat and Dafalias 2008, Liu et al. 2019) stands out for its
- ability to capture the response of these materials under various loading paths, especially cyclic in nature.
- Recently, a model called SANISAND-T (Coulibaly and Rotta Loria 2022) has been proposed to simulate

the mechanics of sands under the influence of monotonic thermal loading, as the primary interest of such investigation consisted in clarifying the contradictory deformation behavior of sands upon heating that affected the state-of-the-art till recent years. As a result of its mathematical formulation, SANISAND-T lacks the capability to simulate thermal cycling effects and would substantially overestimate the plastic deformations associated with thermal cycling effects. Recognizing this limitation, the integration of a "ratcheting control" feature within SANISAND-T becomes imperative to accurately simulate the impact of thermal cycling on the deformation of sands. Notably, this feature represents a key constituent of another model called SANISAND-MS (Liu et al. 2019) that has been presented to simulate the mechanics of sands under the influence of cyclic mechanical loads. This model specifically includes a memory surface to phenomenologically represent micro-mechanical effects associated with fabric changes caused by cyclic loading (e.g., variations in stiffness and dilatancy). Evidence shows that SANISAND-MS can capture in an outstanding manner the magnitude of plastic deformations induced by cyclic mechanical loads (Liu and Pisano 2019), as well as the progressive achievement of terminal densities for such materials – i.e., states where further loading-unloading cycles induce negligible changes in porosity (Narsilio and Santamarina 2008, Chong and Santamarina 2016, Park and Santamarina 2019, 2020, 2023, Cha et al. 2023). Therefore, such a model offers a strong foundation to simulate the mechanics of sands subjected to thermal cycling. Specifically, given the similarities between the (drained) response of sands subjected to cyclic mechanical loads and thermal loads, extending SANISAND-MS to non-isothermal conditions promises to open new opportunities for the detailed simulation of temperature effects in sands.

62

63

64

65

66

67 68

69

70

71 72

73

74

75

76 77

78

79

80

81

82

83

84

85

86

87

88

89

Motivated by the opportunity to enhance the presently limited modeling capabilities of the mechanics of sands under non-isothermal conditions, this paper modifies via a simple yet effective thermo-mechanical coupling the formulation of the SANISAND-MS model, yielding a model that can accurately simulate thermal cycling effects on the mechanics of sands: SANISAND-MS-T. This endeavor provides a modeling tool that can serve the analysis of multiple scientific and engineering problems involving cyclic temperature variations applied to sands and other granular materials, with the ability to expediently explore the influence of myriads thermal cycles and the achievement of a terminal density in such materials – problems that are daunting to address experimentally but can benefit from accelerated computational studies.

2. Methods

91 *2.1. General*

90

- 92 In the following, the key features of the SANISAND-MS model are first presented alongside the thermo-
- 93 mechanical coupling leading to the formulation of the SANISAND-MS-T model. Then, details about the
- 94 implementation of SANISAND-MS-T in a computer routine are provided and information on the
- 95 verification of such implementation is presented. Afterward, details about the validation of SANISAND-
- MS-T are provided. Finally, the features of a sensitivity analysis performed via the SANISAND-MS-T and
- 97 SANISAND-T models to unveil key differences in their modeling capabilities is proposed.
- 98 This paper adopts the geomechanics sign convention. Accordingly, compressive stresses and contractive
- 99 strains are considered positive.

100

101

2.2. Model formulation

- The mathematical formulation of the SANISAND-MS model (Liu et al. 2019) resorts to (i) a yield surface
- f to encompass the elastic domain, (ii) a bounding surface f^B to define current stress bounds based on an
- evolving state parameter, (iii) a dilatancy surface f^D to separate stress regions associated with either
- 105 contractive or dilative deformations, and (iv) a memory surface f^{M} (initially overlapping with yield surface)
- to bounds a stress region evolving with the loading-induced anisotropy in granular fabric. This formulation,
- widely detailed elsewhere (Liu et al. 2019), allows simulating the mechanics of sands under a myriad of
- isothermal mechanical loading paths and account for the stiffening effects caused by drained cyclic loading.
- 109 The SANISAND-MS-T model harnesses the same mathematical formulation of the SANISAND-MS model,
- at the exception of a thermo-mechanical coupling inserted in the total strain decomposition to capture
- thermally induced deformations (i.e., thermal strains). Accordingly, the total strain increment reads:

$$\dot{\varepsilon} = \dot{\varepsilon}^e + \dot{\varepsilon}^p + \dot{\varepsilon}^{th} \tag{1}$$

- where $\dot{\varepsilon}^e$, $\dot{\varepsilon}^p$, and $\dot{\varepsilon}^{th}$ are the increments of elastic strain, plastic strain, and thermal strain, respectively. As
- it is widely accepted in mechanics, the thermal strain is volumetrically given by:

$$\dot{\varepsilon}_{v}^{th} = -\beta \dot{T} \tag{2}$$

- with β the volumetric thermal expansion coefficient of the solid grains (Pan et al. 2020, Coulibaly and Rotta
- Loria 2022) and \dot{T} is the temperature increment. In this context, it is worth noting that despite thermal

strains only involve the diagonal components of the total strain tensor, they not only influence the volumetric response of sands and other materials but also their deviatoric response. This influence primarily depends on the nature of the boundary conditions and/or the presence of non-uniform temperature variations (Laloui and Rotta Loria 2019).

The use of the thermo-mechanical coupling expressed in equation (2), which essentially derives from thermo-elasticity theory (Timoshenko and Goodier 1970, Boley and Weiner 1997), is sufficient to incorporate the effects of temperature variations on the mechanics of sands and other granular materials, as this approach allows reproducing thermally induced strains and thermally induced stresses in such materials. These represent the principal changes in the response of sands subjected to temperature variations relative to isothermal conditions. Notably, the deformation properties of sands appears insensitive to temperature within the range $0 < T < 100^{\circ}$ C (Laloui and Rotta Loria 2019). Additionally, previous experiments on sands highlight that the elastic domain of such materials (in other words, the formulation of their yield surface) also appears insensitive to temperature (Agar 1984, Agar et al. 1986). These materials do experience deformations proportionally to the applied temperature variations and the thermal expansion coefficient of their constituting particles, and undergo thermally induced stresses when any portion of such deformations is restrained. However, the mechanics of sands under non-isothermal conditions is influenced by thermally induced perturbations that are essentially mechanical in nature (Rotta Loria and Coulibaly 2021).

In alignment with the foregoing considerations, the SANISAND-MS-T model integrates the thermomechanical coupling expressed in equation (2) into the formulation of SANISAND-MS with a memory surface. In this work utilizing SANISAND-MS-T, the achievement of a terminal density is considered to obey an empirical relationship between the change in void ratio after successive loading-unloading cycles and the number of cycles (Liu and Pisano 2019, Park and Santamarina 2019):

140
$$e_i = e_T + (e_1 - e_T) \left[1 + \left(\frac{i-1}{N^*} \right)^m \right]^{-1}$$
 (3)

where e_i is the void ratio after i cycles, e_T is the terminal void ratio as $i \to \infty$, e_1 is the void ratio after i = 1 cycle, N^* is the characteristic number of cycles when considering $1 + N^*$ as the required number of cycles for half of the total compaction $(e_1 - e_T)/2$ to occur, and m is a fitted exponent.

Originally, the relationship expressed in equation (3) was proposed to account for the effects of drained cyclic mechanical loads (Liu and Pisano 2019, Park and Santamarina 2019). In this work, such a relationship is considered appropriate to account for the effects of drained cyclic thermal loads because temperature variations in dry and water-saturated sands result in imposed deformations whose effects are

purely physical and comparable to those caused by the application of mechanical forces and displacements (Coulibaly and Rotta Loria 2022). This evidence arguably holds when temperature remains in the range $0 < T < 100^{\circ}$ C because temperature fluctuations within such a range involve negligible thermally induced lubrication effects for particle interactions and, as previously highlighted, lead to negligible thermally induced property changes for the materials that constitute sand particles. Moreover, this evidence is fundamentally different compared to the influence of temperature variations in clays and fine-grained soils at large, whose effects are physico-chemical and greatly differ from those caused by mechanical forces and displacements (Rotta Loria and Coulibaly 2021).

With these premises, the terminal void ratio of sands subjected to thermal cycling can be estimated by fitting the empirical relationship (3). With the estimated terminal density, the maximum change of relative density can finally be calculated as:

$$\Delta D_T = \frac{e_0 - e_T}{e_{max} - e_{min}} \tag{4}$$

where e_{max} and e_{min} are the maximum and minimum attainable void ratios, respectively.

Figure 1 illustrates essential features of the SANISAND-MS-T model in both the triaxial space (Figure 1(a)) and multiaxial space (Figure 1(b)). Table 1 summarizes the mathematical formulation of SANISAND-MS-T in the triaxial and multiaxial stress spaces. Each variable reported is meticulously matched between the two spaces, ensuring a consistent framework where the SANISAND-MS-T and SANISAND-MS models.

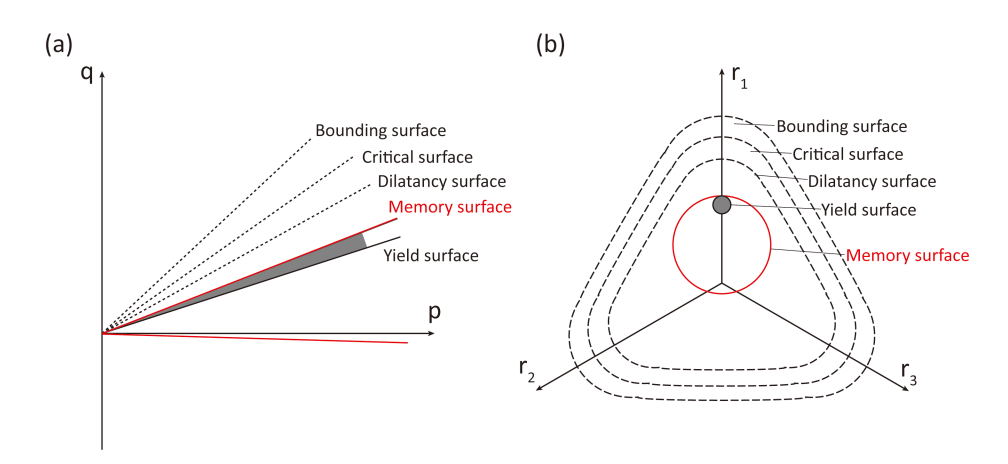


Figure 1: Schematics of the key components of the SANISAND-MS-T model in (a) the triaxial space and (b) the multiaxial space, as originally proposed for the SANISAND-MS model by Liu et al. (2019).

Table 1: Formulation of the SANISAND-MS-T model in the triaxial and multiaxial stress spaces.

	Triaxial formulation	Multiaxial formulation (Liu et al. (2019))
Elastic Moduli	$G = G_0 p_{atm} [(2.97 - e)^2 / (1 + e)] (p/p_{atm})^{1/2}$	$G = G_0 p_{atm} [(2.97 - e)^2 / (1 + e)] (p/p_{atm})^{1/2}$
	K = 2(1+v)G/[3(1-2v)]	K = 2(1+v)G/[3(1-2v)]
Critical state	$e_c = e_0 - \lambda_c (p_c/p_{atm})^{\xi}$	$e_c = e_r - \lambda_c (p_c/p_{atm})^{\xi}$
Yield function	$f = \sqrt{2/3} q - p\alpha - \sqrt{2/3}pm$	$f = \sqrt{(s - p\alpha) : (s - p\alpha)} - \sqrt{2/3}pm$
Memory function	$f^M = \sqrt{2/3} q - p\alpha^M - \sqrt{2/3}pm^M$	$f^{M} = \sqrt{(\mathbf{s} - p\boldsymbol{\alpha}^{M}) : (\mathbf{s} - p\boldsymbol{\alpha}^{M})} - \sqrt{2/3}pm^{M}$
Deviatoric plastic flow	$d\varepsilon_q^p = \sqrt{2/3} \langle L \rangle s$	$de^p = \langle L \rangle R'$
Volumetric plastic flow	$d\varepsilon_v^p = \langle L \rangle D$	$d\varepsilon_v^p = \langle L \rangle D$
	$D = \sqrt{2/3}A_0 \exp\left(\frac{\beta_0(\tilde{b}_d^M)}{b_{ref}}\right)(M^d - \eta)s$	$D = A_0 \exp\left(\frac{\beta_0 \langle \widetilde{b}_d^M \rangle}{b_{ref}}\right) (\boldsymbol{r}_{\theta}^d - \boldsymbol{r}) : \boldsymbol{n}$
	$M^d = sgMexp(n^d \Psi)$	$r_{\theta}^{d} = \sqrt{2/3}g(\theta)Mexp(n^{d}\Psi)\boldsymbol{n}$
	$\tilde{b}_b^M = \sqrt{2/3} (\tilde{M}^d - \tilde{M}^M) s$	$ ilde{b}_b^M = \left(ilde{m{r}}_ heta^d - ilde{m{r}}_ heta^M ight):m{n}$
	$b_{ref} = \sqrt{2/3} M_c^b (1+c)$	$b_{ref} = \left(oldsymbol{r}_{ heta}^b - oldsymbol{r}_{ heta+\pi}^b ight):oldsymbol{n}$
Yield surface evolution	$d\alpha = (2/3)\langle L\rangle h(M^b - \eta)$	$d\boldsymbol{\alpha} = (2/3)\langle L\rangle h(\boldsymbol{r}_{\theta}^b - \boldsymbol{r})$
	$M^b = sgMexp(-n^b\Psi)$	$r_{\theta}^{b} = \sqrt{2/3}g(\theta)Mexp(-n^{b}\Psi)n$
	$h = \frac{b_0}{\sqrt{2/3}(\eta - \eta_{in})s} \exp\left[\mu_0 \left(\frac{p}{p_{atm}}\right)^n \left(\frac{b^M}{b^{ref}}\right)^w\right]$	$h = \frac{b_0}{(\boldsymbol{r} - \boldsymbol{r}_{in}) : \boldsymbol{n}} \exp \left[\mu_0 \left(\frac{p}{p_{atm}} \right)^n \left(\frac{b^M}{b^{ref}} \right)^w \right]$
	$b_0 = G_0 h_0 (1 - c_h e) / \sqrt{p / p_{atm}}$	$b_0 = G_0 h_0 (1 - c_h e) / \sqrt{p/p_{atm}}$
	$b^M = \sqrt{2/3}(M^M - \eta)s$	$b^M = (r^M - r) : n$
Memory surface evolution	$dm^{M} = d\alpha^{M} s - (m^{M}/\zeta) f_{shr} \langle -d\varepsilon_{vol}^{p} \rangle$	$dm^{M} = \sqrt{3/2} d\boldsymbol{\alpha}^{M} : \boldsymbol{n} - (m^{M}/\zeta) f_{shr} \langle -d\varepsilon_{vol}^{p} \rangle$
	$f_{shr} = 1 - \frac{ M^M - \eta + 2m}{2m^M}$	$f_{shr} = 1 - \frac{x_1 + x_2}{x_3}$
	$d\alpha^M = (2/3)\langle L^M \rangle h^M (M^b - M^M)$	$d\boldsymbol{\alpha}^{M} = (2/3)\langle L^{M}\rangle h^{M}(\boldsymbol{r}_{\theta}^{b} - \boldsymbol{r}^{M})$
	$h^{M} = \frac{1}{2} \left[\sqrt{\frac{3}{2} \frac{b_{0}}{(M^{M} - \eta_{in})s}} + \frac{3}{2} \frac{m^{M} f_{shr} \langle -D \rangle}{\zeta (M^{b} - M^{M})s} \right]$	$h^{M} = \frac{1}{2} \left[\frac{b_{0}}{(\boldsymbol{r}^{M} - \boldsymbol{r}_{in}) : \boldsymbol{n}} + \sqrt{\frac{3}{2}} \frac{m^{M} f_{shr} \langle -D \rangle}{\zeta (\boldsymbol{r}_{\theta}^{b} - \boldsymbol{r}^{M}) : \boldsymbol{n}} \right]$

- 172 2.3. Model implementation and verification
- 173 Following its formulation, the SANISAND-MS-T model was implemented in a computer routine by using
- a finite difference method detailed by Coulibaly and Rotta Loria (2022). In this implementation, an explicit
- first-order forward difference is employed along with the method proposed by Bardet and Choucair (1991)
- for imposing the initial and boundary conditions. This approach requires a sufficiently large number of
- explicit time steps to ensure accuracy in the simulations, and such approach is considered in this work.
- Building upon the SANISAND-MS-T model implementation, the correctness of its formulation under
- isothermal conditions was verified by replicating simulations performed with the SANISAND-MS model
- by Liu et al. (2019). These simulations aimed to capture the results of conventional triaxial compression
- tests on quartz sand by Wichtmann (2005) and oedometer tests involving the application of multiple cycles
- of mechanical loading and unloading on Ottawa 50-70 sand by Chong and Santamarina (2016). To ensure
- 183 consistency, the developed verification (Appendix A) resorts to simulations that employed the same
- modeling parameters used by Liu et al. (2019). To ensure accuracy, each triaxial test simulation employed
- 1,000,000 timesteps, and each oedometer test simulation employed 11,000,000 timesteps.

186

187

2.4. Model validation

- Building on the verification of the SANISAND-MS-T model implementation and its ability to capture the
- mechanics of sands under isothermal conditions equally well as the original SANISAND-MS model, a
- validation of the capabilities of SANISAND-MS-T to simulate the response of sands under non-isothermal
- 191 conditions was performed with reference to laboratory experiments on 1 Q-ROK silica sand. Such a sand
- has a chemical composition of over 99% quartz, angular particles, a mean particle size of $D_{50} = 0.48$ mm,
- a coefficient of uniformity $C_u = 1.6$, a maximum void ratio of $e_{max} = 1.049$, a minimum void ratio of
- 194 $e_{min} = 0.708$, and a volumetric thermal expansion coefficient of $\beta = 3.5 \times 10^{-5}$ 1/°C.
- 195 The simulated experiments consisted of the following:
- 196 (i) Conventional triaxial compression tests under isothermal conditions by Leib (2015). In these
- experiments, samples of 1 Q-ROK sand characterized by two different initial void ratios $e_0 = 0.711$ and
- 198 0.907 were tested under two different values of mean effective stress $p'_0 = 69$ and 138 kPa. Shearing was
- imposed by incrementally increasing the axial strain until achieving an axial strain of $\varepsilon_a=25\%$. As some

- of the original data overlapped across varying test conditions, specific test conditions were selected as
- reference.
- 202 (ii) Isothermal oedometer tests involving the application of a single cycle of mechanical loading and
- 203 unloading by Pan et al. (2022). In these experiments, samples of 1 Q-ROK sand under loose and dense
- sands were tested, corresponding to initial void ratios of $e_0 = 0.955$ and 0.766, as well as relative densities
- of $D_R = 27.5\%$ and 80%, respectively. A vertical mechanical stress was incrementally applied under
- laterally restrained conditions from $\sigma_z = 1$ kPa up to $\sigma_z = 1$ MPa, followed by the removal of the applied
- 207 stress back to $\sigma_z = 1$ kPa.
- 208 (iii) Non-isothermal oedometer tests involving the application of a single heating-cooling cycle under
- 209 constant applied vertical stress by Pan et al. (2022). These experiments were performed on virtually
- 210 equivalent samples to those that were tested under isothermal conditions. They involved the mechanical
- preloading of 1 Q-ROK sand through a vertical stress of $\sigma_z = 60$ kPa, followed by the application of one
- heating-cooling cycle with a temperature amplitude of $\Delta T = 60$ °C under constant applied stress.
- 213 (iv) Non-isothermal oedometer tests involving the application of 50 heating-cooling cycles under constant
- applied vertical stress by Pan et al. (2024a). These tests were again performed on loose and dense samples
- of 1 Q-ROK sand. They involved the mechanical preloading of 1 Q-ROK sand through a vertical stress of
- $\sigma_z = 60$ kPa, followed by the application of 50 thermal cycles with a temperature amplitude of $\Delta T = 60$ °C
- 217 under constant applied stress.
- In order to simulate all these experiments, it was necessary to calibrate the 16 constitutive parameters
- characterizing the SANISAND-MS-T model (Table 2). Such a calibration followed a similar approach to
- the one employed by Liu et al. (2019) and Dafalias and Manzari (2004). The parameters from G_0 to n^d (i.e.,
- 221 13 parameters) were calibrated to fit the deviatoric stress-axial strain $(q-\varepsilon_a)$ and volumetric strain-axial
- strain $(\varepsilon_v \varepsilon_a)$ plots obtained from the results of monotonic triaxial tests (i.e., experiments (i)), while the
- remaining ones (i.e., 3 parameters) governing the memory surface were calibrated from the results of cyclic
- loading tests (i.e., experiments (iv)).
- 225 All simulations considered a representative volume element under quasistatic conditions. The simulations
- of the isothermal tests leveraged 1,000,000 timesteps to ensure accuracy, whereas those of the non-
- 227 isothermal tests used 80,000 timesteps for every 60°C of applied temperature variation. Sensitivity analyses
- 228 were conducted to verify that such numbers of timesteps allowed to maintain accuracy and control errors
- effectively. For instance, in sensitivity analyses comparing simulations of 50 thermal cycles to those using
- 230 1,000,000 timesteps for every 60 °C, the error was regulated within 0.01% of the strain magnitude.

Table 2: Constitutive parameter calibrated for the 1 Q-ROK silica sand.

Elast	icity	Critical state					Yield surface	Plas	tic mod	ulus	Dilat	ancy	Men	nory sur	face
G_0	υ	М	С	λ_c	e_r	ξ	m	h_0	$c_{\rm h}$	n^b	A_0	n^d	μ_0	ζ	β_0^*
230	0.1	1.42	0.75	0.01	0.928	0.7	0.05	1.7	0.85	1.3	0.6	1.6	635	0.005	1

^{*}To avoid conflicts of symbol notation, β_0 and e_r correspond to the β and e_0 , respectively, in the original SANISAND-MS model.

2.5. Sensitivity analyses

In addition to the validation of the capability of SANISAND-MS-T to simulate the influence of a relatively limited number of thermal cycles on the mechanics of sands (i.e., 50 cycles), this work also tested the performance of the considered model in the simulation of a significantly larger number of thermal cycles (i.e., 10,000). This endeavor had a twofold purpose: on the one hand, compare the predictions of the SANISAND-MS-T and SANISAND-T for a large number of thermal cycles applied to sands; on the other hand, explore the evolutionary deformations of sands till the achievement of terminal densities due to thermal cycling – a study that may be achieved via laboratory experiments within a reasonable time for cyclic mechanical loads, but is infeasible for cyclic thermal loads due to the markedly longer time required to gather reliable measurements.

The comparison between the capabilities of SANISAND-MS-T and SANISAND-T was based on simulations that referred to the same initial conditions, relative densities, stress level, and temperature amplitude characterizing the experiments (iv) described in Section 2.4. In this context, the simulations performed with SANISAND-MS-T used the entire 16 constitutive parameters reported in Table 2 and fitted the empirical relationship reported in equation (3) with the parameters listed in Table 3. As no memory surface characterizes the SANISAND-T model, the simulations performed with this model used only the first 13 parameters reported in Table 2. Additionally, as no particle breakage was involved in the experiments, the cap of the yield surface in the SANISAND-T simulations was configured with parameters that ensured negligible impacts on the simulation results.

The exploration of the achievement of a terminal density in sands subjected to a large number of thermal cycles was based on simulations with the SANISAND-MS-T model, which considered the same problems mentioned above but analyzed the influence of two temperature amplitudes $\Delta T = 30$ and 60°C.

Table 3: Estimated terminal density e_T *and fitted parameters of the empirical relationship.*

Initial relative density	Δ <i>T</i> [°C]	e_T [-]	N* [-]	m [-]
Loose	60	0.915	134	0.3
Dense	60	0.765	90	0.3
Loose	30	0.935	2000	0.3
Dense	30	0.768	781	0.3

3. Results and discussion

3.1. General

This section is divided in two parts. First, the section addresses an overview of the simulation capabilities of the SANISAND-MS-T model. Next, the section presents a comparison between simulation results obtained via the SANISAND-MS-T and SANISAND-T models, as well as an analysis of the achievement of terminal densities in sands subjected to a large number of thermal cycles.

3.2. Validation of SANISAND-MS-T capabilities

Figure 2 presents a comparison between the results of drained triaxial tests performed by Leib (2015) and SANISAND-MS-T simulations. The results indicate a satisfactory agreement between the simulation and the experimental data, both in terms of deviatoric stress against axial strain (Figure 2(a) and (c)) as well as in terms of volumetric strain against axial strain (Figure 2(b) and (d)). The results particularly support that the calibrated SANISAND-MS-T simulations can capture well the response of 1 Q-ROK sand to isothermal monotonic mechanical loading under drained triaxial conditions. This evidence holds for variable levels of mean effective stress and different initial void ratios.

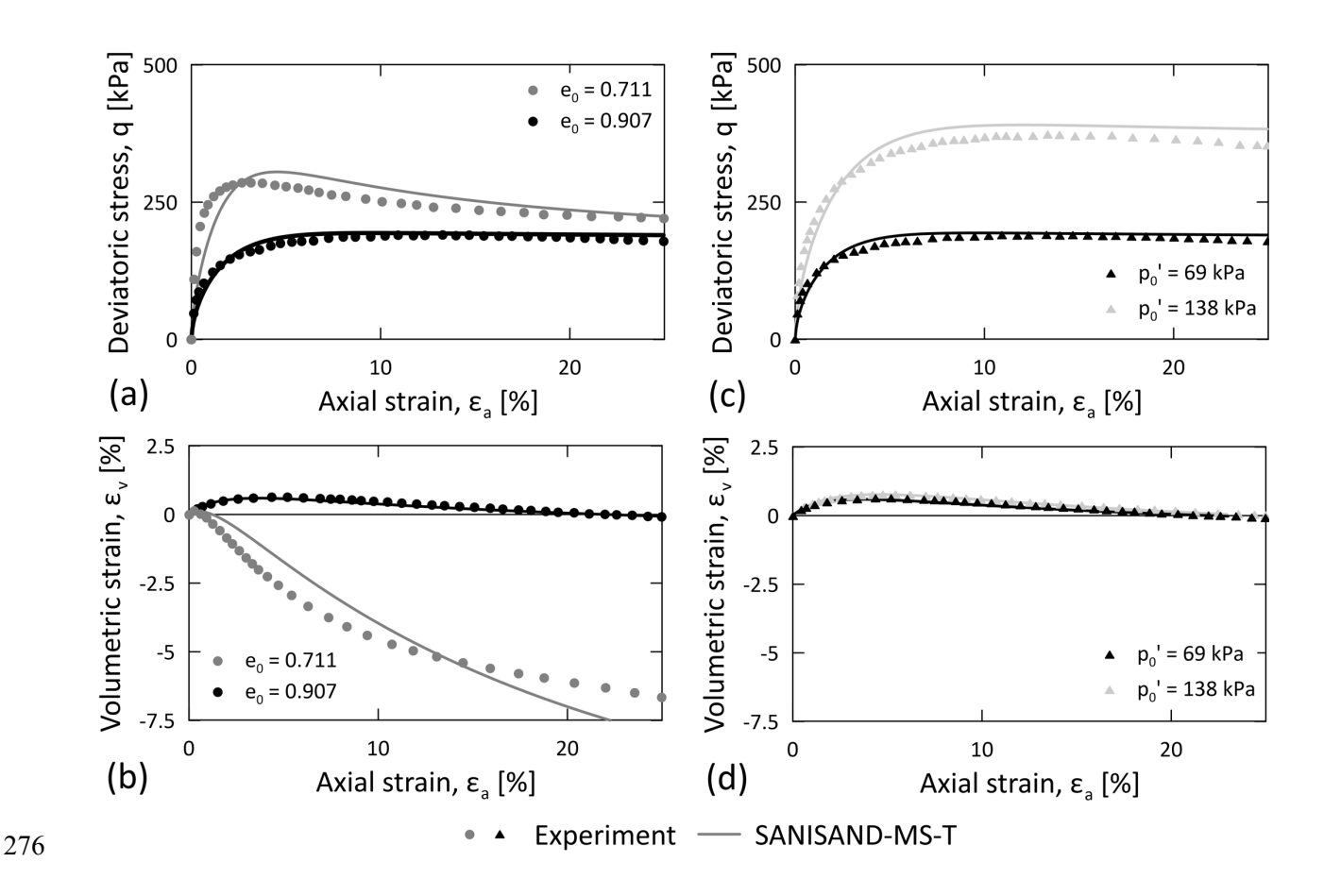


Figure 2: Validation of SANISAND-MS-T model capabilities against the results of drained triaxial tests on 1 Q-ROK silica sand performed by Leib (2015). (a) $q - \varepsilon_a$ plots and (b) $\varepsilon_v - \varepsilon_a$ plots for a constant initial mean effective stress of $p_0' = 69$ kPa and different initial void ratios e_0 , and (c) $q - \varepsilon_a$ plots and (d) $\varepsilon_v - \varepsilon_a$ plots for a constant initial void ratio of $e_0 = 0.907$ and different initial values of mean effective stress p_0' .

Figure 3 presents a comparison between the results of isothermal oedometer tests reported by Pan et al. (2024a) and SANISAND-MS-T simulations. The results indicate that SANISAND-MS-T can capture with some discrepancies the response of the tested 1 Q-ROK sand subjected to isothermal mechanical loading and unloading under oedometric conditions. The results particularly show that the SANISAND-MS-T simulations accurately predict the experimental data during the loading process but are affected by discrepancies during the unloading process, irrespective of whether the sand is loose (Figure 3(a)) or dense (Figure 3(b)). These discrepancies result in considerably smaller plastic deformations observed at the end of the loading-unloading process in the simulations as compared to the experiments. As shown in Appendix A, a similar discrepancy affected SANISAND-MS simulations when considering the first cycle of mechanical loading and unloading in the tests performed by Chong and Santamarina (2016), although the

cyclic response of the tested sand was eventually captured well over 100 cycles of mechanical loading and unloading. It is important to note that the calibration of the first 13 parameters of SANISAND-MS-T and SANISAND-MS (based on the monotonic drained triaxial tests) only serves the simulation of loading processes, but not unloading processes. Therefore, the simulation of unloading processes could be improved by adjusting the plastic modulus and dilatancy. However, the results would then exhibit larger differences from the data referring to monotonic loading processes (e.g., the drained triaxial tests reported in Figure 2).

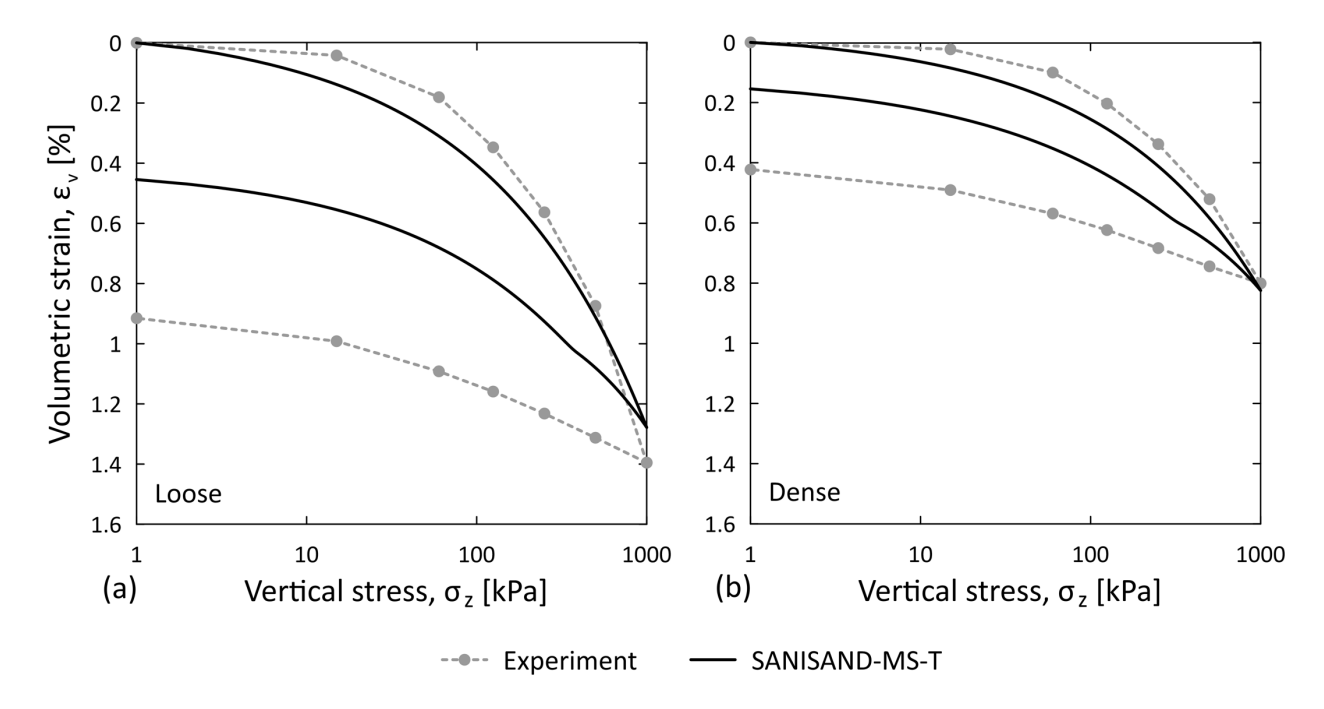


Figure 3: Validation of SANISAND-MS-T model capabilities against the results of loading-unloading oedometer tests on 1 Q-ROK silica sand performed by Pan et al. (2024a) in terms of $\varepsilon_v - \sigma_z$ plots. (a) Loose condition with initial void ratio of $e_0 = 0.955$. (b) Dense condition with initial void ratio of $e_0 = 0.776$.

Figure 4 show a comparison between the results of non-isothermal oedometer tests involving the application of one heating-cooling cycle to loose and dense samples of 1 Q-ROK sand by Pan et al. (2022) and SANISAND-MS-T simulations. A detailed comparison within the first heating-cooling cycle with measurements reaching thermal equilibrium at varying temperature steps is provided. The results demonstrate that the simulation data compare well with the experimental results. Notably, the simulation results closely align with the average trend of the experimental results during heating and capture the irreversible deformation after the one heating-cooling cycle. Although the simulated cooling (unloading)

phase does not perfectly match the experimental data, it remains within an acceptable margin defined by the error bars (i.e., the shaded regions). This result highlights the effectiveness of the thermo-mechanical coupling employed in SANISAND-MS-T with equations (2) and (3) to capture the thermally induced deformations of sands upon one heating-cooling cycle.

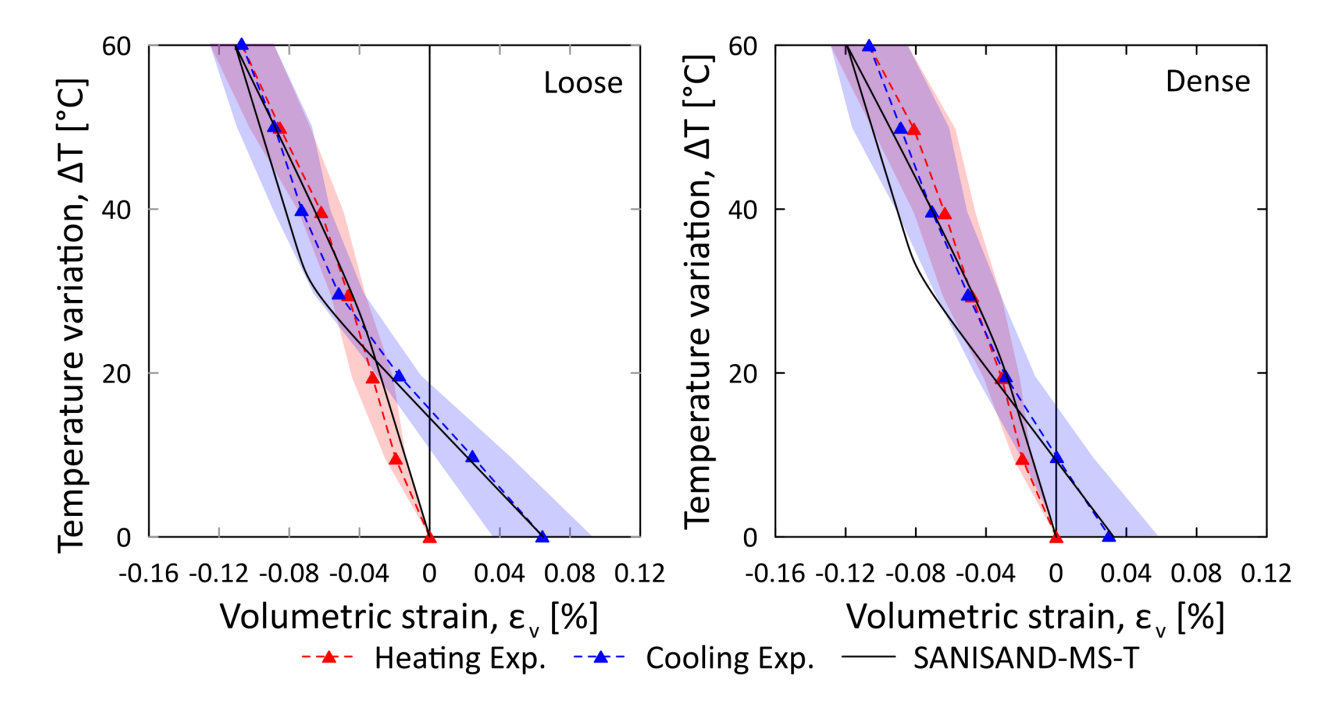


Figure 4: Validation of SANISAND-MS-T model capabilities against the results of non-isothermal oedometer tests performed by Pan et al. (2022), involving the application of one heating-cooling cycle to 1 Q-ROK silica sand. $\Delta T - \varepsilon_v$ plots for a (a) loose condition with initial void ratio of $e_0 = 0.955$ and a (b) dense condition with initial void ratio of $e_0 = 0.776$.

Figure 5 show a comparison between the results of non-isothermal oedometer tests involving the application of one heating-cooling cycle to loose and dense samples of 1 Q-ROK sand by Pan et al. (2024a) and SANISAND-MS-T simulations. The results support that SANISAND-MS-T can accurately model the evolution of thermally induced volumetric strains of 1 Q-ROK sand subjected to 50 heating-cooling cycles. This evidence proves the capability of SANISAND-MS-T to simulate the volumetric expansion upon heating and volumetric contraction upon cooling, as well as the accumulation of plastic deformations at the end of each thermal cycle under loose (Figure 5(a)) and dense (Figure 5(b)) conditions. These results demonstrate the capability SANISAND-MS-T in modeling thermal cycling effects in addition to mechanical cycling effects.

Only minor limitations can be identified for the performance of SANISAND-MS-T in simulating the cyclic thermally induced deformation of sands (Figure 5(c)). For example, the SANISAND-MS-T model predicts a slightly larger magnitude of expansion upon most heating paths than the experimental data. These limitation may be associated with the several factors including heating rates and particle shapes (Pan et al. (2024a). Although the consideration of these effects may be possible through a further modification of the mathematical formulation of SANISAND-MS-T, such an endeavor is not addressed in this work mainly because the increase in complexity that would characterize the mathematical formulation of such a new version of SANISAND-MS-T would not be commensurate with the added accuracy to its simulation results.

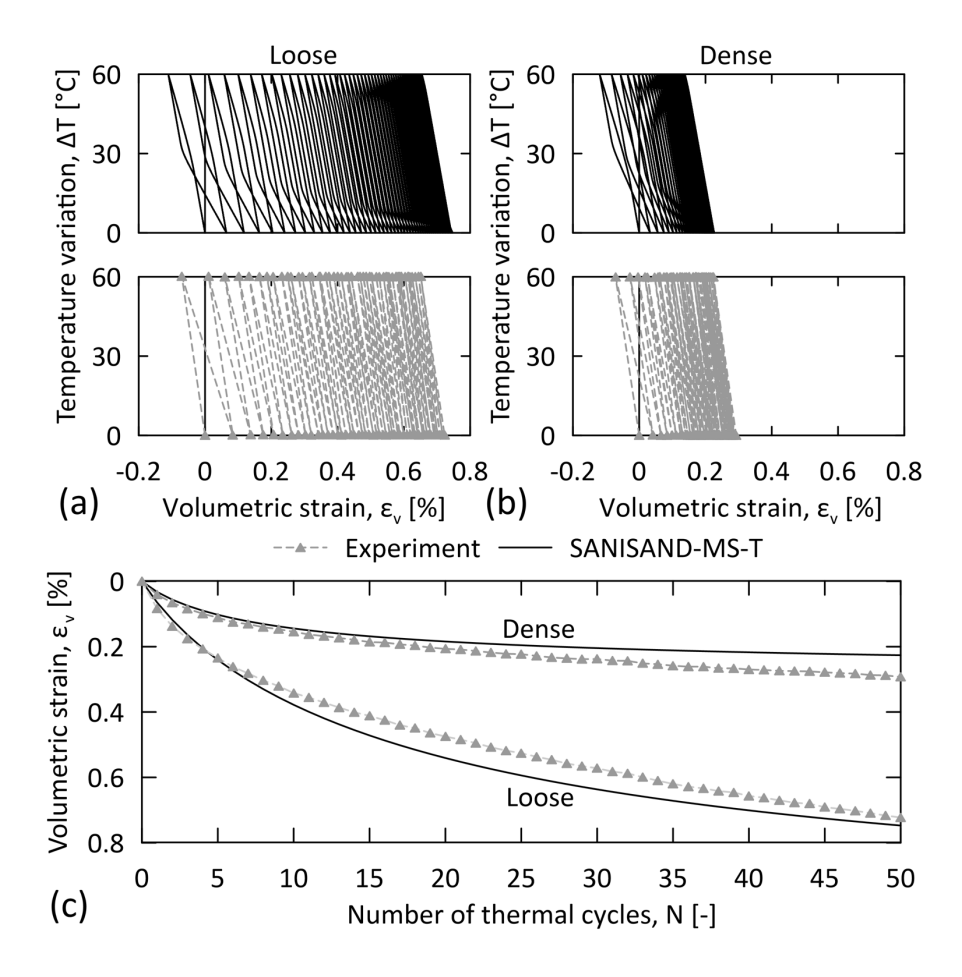


Figure 5: Validation of SANISAND-MS-T model capabilities against the results of thermal cycling oedometer tests on 1 Q-ROK silica sand performed by Pan et al. (2024a). $\Delta T - \varepsilon_v$ plots for a (a) loose condition with initial void ratio of $e_0 = 0.955$ and a (b) dense condition with initial void ratio of $e_0 = 0.776$.(c) $\varepsilon_v - N$ plots for both loose and dense conditions.

3.3. Sensitivity analyses via SANISAND-MS-T and SANISAND-T

Figure 6 presents the results of sensitivity analyses that apply 10,000 thermal cycles to 1 O-ROK sand under constant applied stress. Specifically, Figure 6(a) shows a comparison between SANISAND-T and SANISAND-MS-T simulation results in terms of the evolution of void ratio against the number of applied thermal cycles with a temperature amplitude of $\Delta T = 60^{\circ}$ C, whereas Figure 6(b) shows the maximum change in relative density at terminal density against the initial relative density provided by SANISAND-

MS-T simulation data after 10,000 thermal cycles.

348

349

350

351 352

353 354

355

356

357

358

359

360

361

362

363 364

365

366

367 368

369

370

As can be noted in Figure 6(a), the SANISAND-T simulations significantly overestimate the change in void ratio due to thermal cycling for sands under both loose and dense conditions. The void ratio obtained through the SANISAND-T simulations particularly deviates from the experimental data during the first 50 thermal cycles and reaches zero even before completing 10,000 thermal cycles. In contrast, the SANISAND-MS-T simulations effectively capture the evolution of void ratio, closely aligning with the experimental data during the initial 50 thermal cycles. The SANISAND-MS-T simulations further reveal a progressive reduction in plastic strains after each successive thermal cycle, reaching a terminal density that is not associated with a void ratio of zero as the number of thermal cycles increases $(N \to \infty)$. The comparison between the results of SANISAND-T and SANISAND-MS-T simulations highlights the enhanced performance of the SANISAND-MS-T model in simulating thermal cycling effects in sand compared to SANISAND-T. This enhanced performance of SANISAND-MS-T in capturing thermal cycling effects in sands is due to the incorporation of the memory surface. The blue dotted lines in Figure 6(a) show the expansion of the memory surface in response to the application of thermal cycles. This feature effectively accounts for the stiffening effect due to cyclic loading and contributes significantly to the model capability to capturing the cyclic response of the modeled material.

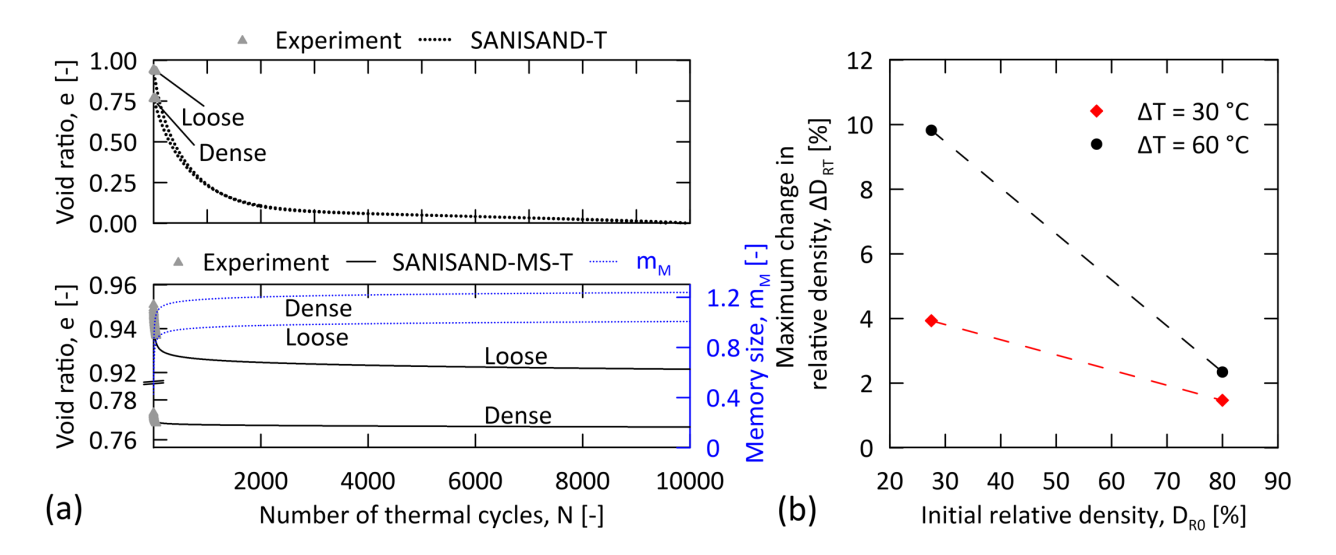


Figure 6: Sensitivity analyses considering 10,000 thermal cycles. (a) Comparison of e-N plots between the SANISAND-MS-T and SANISAND-T model results with $\Delta T=60$ °C. (b) $\Delta D_{RT}-D_{R0}$ plots for the SANISAND-MS-T results.

As can be noted in Figure 6(b), a larger change in relative density due to thermal cycling is achieved for a lower initial relative density or a larger temperature amplitude. Depending on the initial relative density and the temperature amplitude, the change in relative density due to thermal cycling can exceed the significant value of 10%. Although this value is achieved in the present simulations for a loose sand subjected to 10,000 cycles with a temperature amplitude of $\Delta T = 60^{\circ}$ C after the application of such a large number of cycles, a very similar value is already obtained after only about 2000 thermal cycles. This result corroborates that thermal cycling can lead to significant changes in void ratio and relative density in sands. Such changes specifically appear comparable to those achievable as a result of mechanical cycling (Chong and Santamarina 2016, Park and Santamarina 2019).

4. Concluding remarks

Motivated by the lack of constitutive models to capture thermal cycling effects in granular materials such as sands, this paper extended the SANISAND-MS model with a thermo-mechanical coupling to capture thermal cycling effects in sands, leading to the formulation of SANISAND-MS-T: a Simple ANIsotropic SAND model with Memory Surface for Temperature effects. A comparison between various experimental data with SANISAND-MS-T model simulations allows drawing the following main conclusions:

- 1) The SANISAND-MS-T model represents an extended version of the SANISAND-MS model for simulating the mechanics of sands under non-isothermal conditions.
- The SANISAND-MS-T model realistically captures the influence of both mechanical and thermal loads,
 irrespective of whether these loads are monotonic and cyclic in nature.
- 396 3) The SANISAND-MS-T model has difficulties in accurately reproducing the experimentally observed deformation of sands when they are mechanically or thermally unloaded for the first time but allows to simulate accurately and effectively the experimentally observed deformation of sands when they are subsequently subjected to further cycles during both loading and unloading.
- 400 4) The SANISAND-MS-T model represents a powerful tool to study the mechanics of sands under the influence of multiple mechanical and thermal cycles of loading and unloading, which excels in quantifying the plastic volumetric deformations in such materials caused by mechanical and thermal cycling effects.
 - 5) The SANISAND-MS-T model predicts that both mechanical and thermal cyclic loads can lead to the achievement of a terminal density in sands. This feature of the model makes it suitable to simulate multiple scientific engineering problems where sands and other granular materials are subjected to a myriad of mechanical and/or thermal cycles. This tool is considered particularly valuable due to the substantial time required by laboratory experiments to analyze cyclic loading effects on the mechanics of sands.

404405

406407

408

409

411

412

416

417

418

419

420

421

422

5. Appendix A

- This appendix presents the simulation results to verify the implementation of SANISAND-MS-T against the original results of SANISAND-MS model. The verification includes the results of drained triaxial tests and oedometer tests.
 - Figure 7 presents a comparison between the results of drained triaxial tests reported by Wichtmann (2005) and SANISAND-MS-T simulations. The results indicate that SANISAND-MS-T can capture the response of the tested quartz sand subjected to isothermal monotonic mechanical loading under drained triaxial conditions, both in terms of deviatoric stress against axial strain (Figure 7(a) and (c)) as well as in terms of volumetric strain against axial strain (Figure 7(b) and (d)). This evidence holds for variable levels of mean effective stress and different initial void ratios (corresponding to variable relative densities), with minimal differences between the simulation and experimental results. The simulation results particularly support

that SANISAND-MS-T can capture key features of the response of sands subjected to shearing: increased strength for a higher relative density and a higher mean effective stress, contractive and dilatancy response under loose and dense conditions, respectively, as well as peak and constant volume strength for relatively limited and large values of strain, respectively.

Figure 8 presents a comparison between the results of oedometer tests reported by Chong and Santamarina (2016), SANISAND-MS simulations reported by Liu et al. (2019), and SANISAND-MS-T simulations. The results indicate that SANISAND-MS-T can capture the experimentally observed response of the tested Ottawa 50-70 sand subjected to isothermal cyclic mechanical loading under oedometric conditions (Figure 8(a)). These results particularly confirm the consistency between the results achieved with the formulations of SANISAND-MS (Figure 8(b)) and SANISAND-MS-T (Figure 8(c)), and verify the suitability of SANISAND-MS-T in accurately capturing the mechanics of sands under cyclic mechanical loading. Although minor deviations exist between the reference simulation results and those obtained in this work, such deviations are attributed to the different implementation methods of the SANISAND-MS and SANISAND-MS-T models (i.e., a finite element implementation in the reference study as opposed to a single material point implementation in this work).

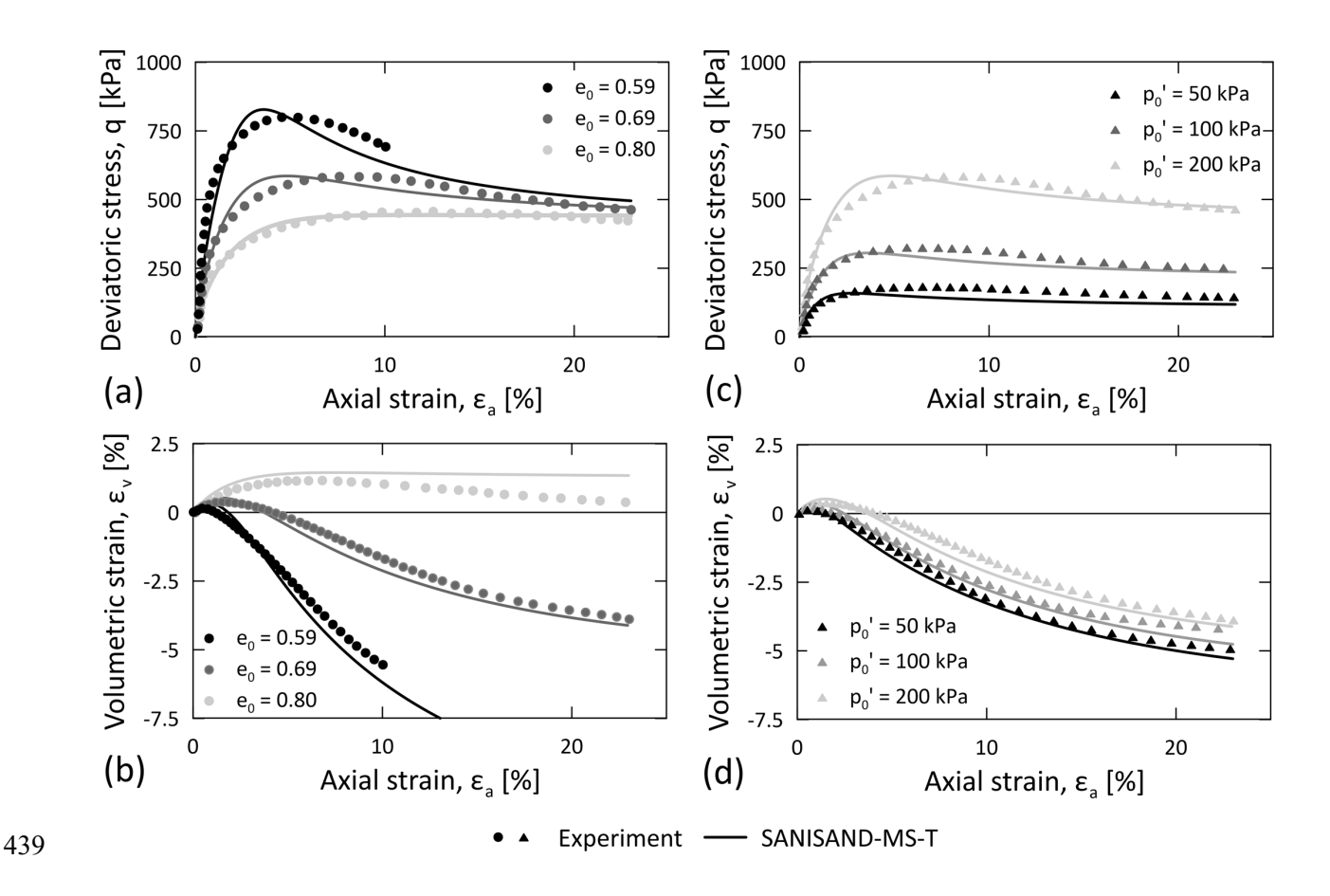


Figure 7: Verification of SANISAND-MS-T model implementation against the results of drained triaxial tests on quartz sand performed by Wichtmann (2005). (a) $q - \varepsilon_a$ plots and (b) $\varepsilon_v - \varepsilon_a$ plots for a constant initial mean effective stress of $p_0' = 200$ kPa and different initial void ratios e_0 , and (c) $q - \varepsilon_a$ plots and (d) $\varepsilon_v - \varepsilon_a$ plots for a constant initial void ratio of $e_0 = 0.69$ and different initial values of mean effective stress p_0' . The SANINSAND-TC simulations employed the same parameter input parameters as those considered by Liu et al. (2019).

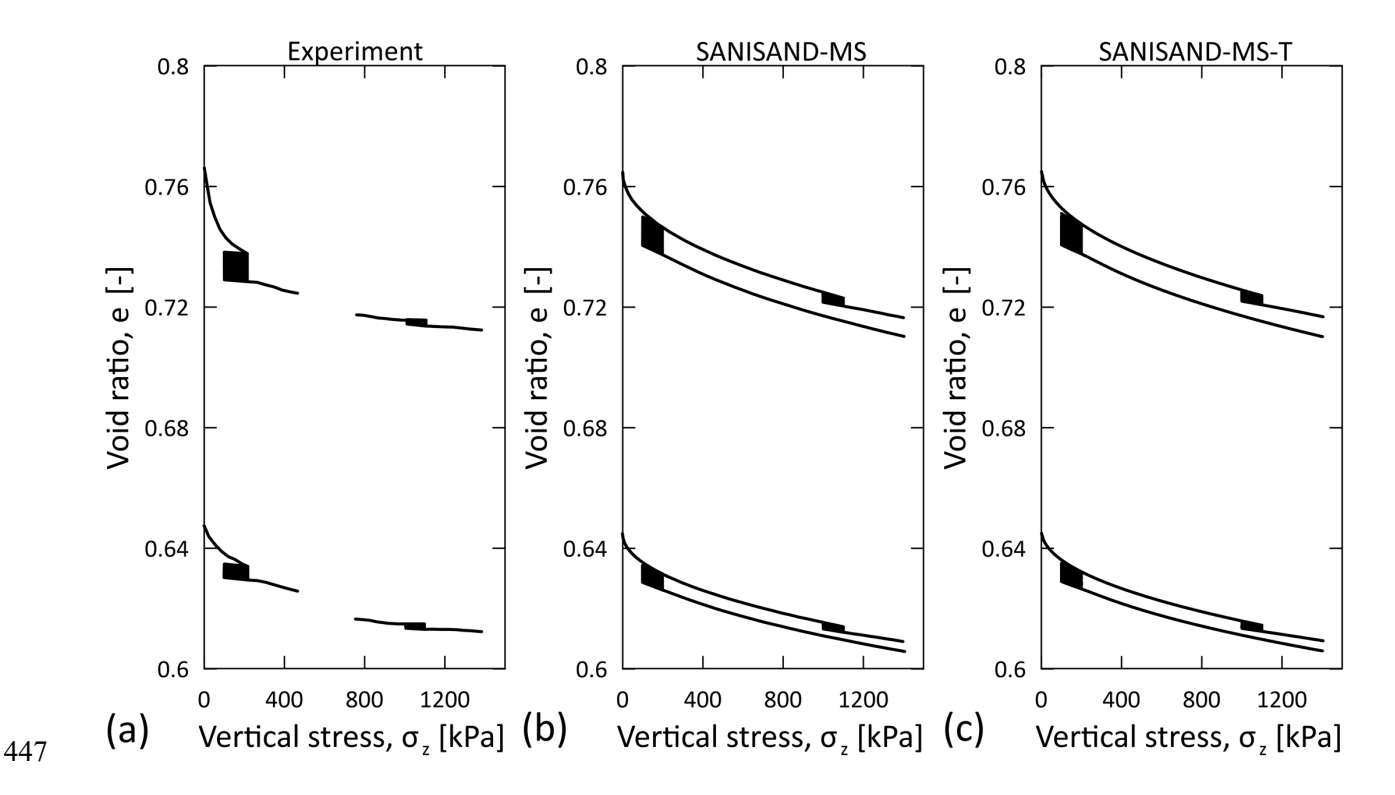


Figure 8: Verification of SANISAND-MS-T model implementation against the results of cyclic oedometer tests on Ottawa 50-70 sand performed by Chong and Santamarina (2016) and the results of SANISAND-MS simulations obtained by Liu et al. (2019) in terms of $e-\sigma_z$ plots. (a) Reference experimental data; (b) Reference simulation data; and (c) present simulation results. The SANINSAND-TC simulations employed the same parameter input parameters as those considered by Liu et al. (2019).

Acknowledgements

This research was supported by the National Science Foundation (project grant No. 2046586).

References

- Agar, J.G. 1984. Geotechnical behaviour of oil sands at elevated temperatures and pressures. Ph.D. Thesis, Univerity of Alberta, Edmonton, Alberta, Canada.
- Agar, J.G., Morgenstern, N.R., and Scott, J.D. 1986. Thermal-expansion and pore pressure generation in oil sands. Canadian Geotechnical Journal, **23**(3): 327–333.
- Bardet, J.P., and Choucair, W. 1991. A linearized integration technique for incremental constitutive equations. International Journal for Numerical and Analytical Methods in Geomechanics, **15**(1): 1–19. doi:10.1002/nag.1610150102.
- Boley, B.A., and Weiner, J.H. 1997. Theory of thermal stresses. Dover Publications, Mineola, New York, United States of America.

- Carson, J.W. 2001. Silo failures: Case histories and lessons learned. Handbook of Powder Technology, **10**: 153–166.
- Cha, W., Park, J., and Santamarina, J.C. 2023. Long-Term Response of Sand Subjected to Repetitive Simple
 Shear Loading: Shakedown, Ratcheting, and Terminal Void Ratio. Journal of Geotechnical and
 Geoenvironmental Engineering, **149**(6): 04023028. American Society of Civil Engineers.
- Chen, K., Cole, J., Conger, C., Draskovic, J., Lohr, M., Klein, K., Scheidemantel, T., and Schiffer, P. 2006.
 Granular materials: Packing grains by thermal cycling. Nature, **442**(7100): 257.

475

476 477

478

479

480

481 482

483

484

485 486

487

488

489

490

491

492

493

494

495 496

502

- Chong, S.-H., and Santamarina, J.C. 2016. Sands subjected to repetitive vertical loading under zero lateral strain: accumulation models, terminal densities, and settlement. Canadian Geotechnical Journal, 53(12): 2039–2046. NRC Research Press. doi:10.1139/cgj-2016-0032.
- Coulibaly, J.B., and Rotta Loria, A.F. 2022. Transient dynamics of the thermally induced deformation of sands. International Journal for Numerical and Analytical Methods in Geomechanics, **46**(10): 1972–1988. Wiley Online Library.
- Coulibaly, J.B., Shah, M., and Rotta Loria, A.F. 2020. Thermal cycling effects on the structure and physical properties of granular materials. Granular Matter, **22**(4): 80. doi:10.1007/s10035-020-01054-6.
- Dafalias, Y.F., and Manzari, M.T. 2004. Simple Plasticity Sand Model Accounting for Fabric Change Effects. Journal of Engineering Mechanics, **130**(6): 622–634. American Society of Civil Engineers. doi:10.1061/(ASCE)0733-9399(2004)130:6(622).
- Dogangun, A., Karaca, Z., Durmus, A., and Sezen, H. 2009. Cause of Damage and Failures in Silo Structures. Journal of Performance of Constructed Facilities, **23**(2): 65–71. American Society of Civil Engineers. doi:10.1061/(ASCE)0887-3828(2009)23:2(65).
- Dreissigacker, V., Müller-Steinhagen, H., and Zunft, S. 2010. Thermo-mechanical analysis of packed beds for large-scale storage of high temperature heat. Heat and Mass Transfer, **46**(10): 1199–1207. doi:10.1007/s00231-010-0684-5.
- He, S.-H., Shan, H.-F., Xia, T.-D., Liu, Z.-J., Ding, Z., and Xia, F. 2021. The effect of temperature on the drained shear behavior of calcareous sand. Acta Geotechnica, **16**(2): 613–633. doi:10.1007/s11440-020-01030-7.
- Iliev, P.S., Giacomazzi, E., Wittel, F.K., Mendoza, M., Haselbacher, A., and Herrmann, H.J. 2019. Behavior of confined granular beds under cyclic thermal loading. Granular Matter, **21**(3): 59. doi:10.1007/s10035-019-0914-6.
- Kong, G., Fang, J., Huang, X., Liu, H., and Abuel-Naga, H. 2021. Thermal induced horizontal earth pressure changes of pipe energy piles under multiple heating cycles. Geomechanics for Energy and the Environment, **26**: 100228. doi:10.1016/j.gete.2020.100228.
- Kosar, K.M. 1983. The effect of heated foundations on oil sand. Master's Thesis, University of Alberta, Edmonton, Alberta, Canada.
 - Laloui, L., and Rotta Loria, A.F. 2019. Analysis and Design of Energy Geostructures: Theoretical Essentials and Practical Application. Academic Press.
- Lee, K.S. 2013. Underground Thermal Energy Storage. *In* Underground Thermal Energy Storage. *Edited by* K.S. Lee. Springer London, London. pp. 15–26.
- Leib, A.R. 2015. Effect of particle morphology on the deformation behavior of sand under monotonic loading conditions.
- Liu, H., McCartney, J.S., and Xiao, Y. 2020. Thermal volume changes of saturated sand during loadingunloading-heating phase. E3S Web of Conferences, **205**: 08002. doi:10.1051/e3sconf/202020508002.
- Liu, H., and Pisano, F. 2019. Prediction of oedometer terminal densities through a memory-enhanced cyclic model for sand. Géotechnique Letters, **9**(2): 81–88. Thomas Telford Ltd.
- Liu, H., Xiao, Y., McCartney, J.S., and Liu, H. 2018. Influence of temperature on the volume change behavior of saturated sand. Geotechnical Testing Journal, **41**(4).

- Liu, H.Y., Abell, J.A., Diambra, A., and Pisanò, F. 2019. Modelling the cyclic ratcheting of sands through memory-enhanced bounding surface plasticity. Géotechnique, **69**(9): 783–800. Thomas Telford Ltd.
- Manbeck, H.B. 1984. Predicting thermally induced pressures in grain bins. Transactions of the ASAE, **27**(2): 0482–0486.
- Mitterlehner, T., Kartnig, G., and Haider, M. 2020. Analysis of the thermal ratcheting phenomenon in packed-bed thermal energy storage using Discrete Element Method. FME Transactions, **48**(2): 427–431.
- Narsilio, A., and Santamarina, J.C. 2008. Terminal densities. Geotechnique, **58**(8): 669.

536

537

538

539

540

541

542

543544

545

546

547

548

549

550

551

552553

554

- Ng, C.W.W., Ma, Q.J., and Gunawan, A. 2016a. Horizontal stress change of energy piles subjected to thermal cycles in sand. Computers and Geotechnics, **78**: 54–61.
- Ng, C.W.W., Wang, S.H., and Zhou, C. 2016b. Volume change behaviour of saturated sand under thermal cycles. Géotechnique Letters, **6**(2): 124–131.
- Pan, Y., Coulibaly, J.B., and Rotta Loria, A.F. 2020. Thermally induced deformation of coarse-grained soils under nearly zero vertical stress. Géotechnique Letters, **10**(4): 486–491. doi:10.1680/jgele.20.00013.
- Pan, Y., Coulibaly, J.B., and Rotta Loria, A.F. 2022. An experimental investigation challenging the thermal collapse of sand. Géotechnique,: 1–27. Thomas Telford Ltd.
- Pan, Y., Gong, X., and Rotta Loria, A.F. 2024a. Thermal ratcheting in granular materials with irregular particle shapes. Scientific Reports, **under review**. doi:10.21203/rs.3.rs-3108175/v1.
 - Pan, Y., Seo, D., Rivers, M., Gong, X., Buscarnera, G., and Rotta Loria, A.F. 2024b. Mechanistic insights into the thermal ratcheting of granular materials. Granular Matter, **under review**.
 - Park, J., and Santamarina, J.C. 2019. Sand response to a large number of loading cycles under zero-lateral-strain conditions: evolution of void ratio and small-strain stiffness. Géotechnique, **69**(6): 501–513. Thomas Telford Ltd.
 - Park, J., and Santamarina, J.C. 2020. Soil Response to Repetitive Changes in Pore-Water Pressure under Deviatoric Loading. Journal of Geotechnical and Geoenvironmental Engineering, **146**(5): 04020023. American Society of Civil Engineers. doi:10.1061/(ASCE)GT.1943-5606.0002229.
 - Park, J., and Santamarina, J.C. 2023. Sands Subjected to Repetitive Loading Cycles and Associated Granular Degradation. Journal of Geotechnical and Geoenvironmental Engineering, **149**(11): 04023111. doi:10.1061/JGGEFK.GTENG-11153.
 - Percier, B., Divoux, T., and Taberlet, N. 2013. Insights on the local dynamics induced by thermal cycling in granular matter. EPL (Europhysics Letters), **104**(2): 24001. doi:10.1209/0295-5075/104/24001.
 - Rotta Loria, A.F., and Coulibaly, J.B. 2021. Thermally induced deformation of soils: a critical overview of phenomena, challenges and opportunities. Geomechanics for Energy and the Environment,: 100193.
 - Sassine, N., Donzé, F.-V., Harthong, B., and Bruch, A. 2018. Thermal stress numerical study in granular packed bed storage tank. Granular Matter, **20**(3). doi:10.1007/s10035-018-0817-y.
 - Sittidumrong, J., Jotisankasa, A., and Chantawarangul, K. 2019. Effect of thermal cycles on volumetric behaviour of Bangkok sand. Geomechanics for Energy and the Environment,: 100127. doi:10.1016/j.gete.2019.100127.
- Taiebat, M., and Dafalias, Y.F. 2008. SANISAND: Simple anisotropic sand plasticity model. International Journal for Numerical and Analytical Methods in Geomechanics, **32**(8): 915–948. doi:10.1002/nag.651.
- Timoshenko, S., and Goodier, J. 1970. Theory of elasticity. McGraw-Hill, New York.
- Vargas, W.L., and McCarthy, J.J. 2007a. Thermal expansion effects and heat conduction in granular materials. Physical Review E, **76**(4). doi:10.1103/physreve.76.041301.
- Vargas, W.L., and McCarthy, J.J. 2007b. Thermal expansion effects and heat conduction in granular materials. Physical Review E, **76**(4): 041301. doi:10.1103/physreve.76.041301.

- Wang, C., Liu, H., Kong, G., and Wang Wai Ng, C. 2017. Different types of energy piles with heating—cooling cycles. Proceedings of the Institution of Civil Engineers Geotechnical Engineering, 170(3): 220–231. ICE Publishing. doi:10.1680/jgeen.16.00061.
- Wichtmann, T. 2005. Explicit accumulation model for non-cohesive soils under cyclic loading. Inst. für Grundbau und Bodenmechanik Braunschweig, Germany.
- Yavari, N., Tang, A.M., Pereira, J.-M., and Hassen, G. 2014. Experimental study on the mechanical behaviour of a heat exchanger pile using physical modelling. Acta Geotechnica, **9**(3): 385–398.
 - Zhao, N., Cheng, X., and Whittle, A.J. 2022a. Extended TTS Model for Thermal and Mechanical Creep of Clay and Sand. Journal of Geotechnical and Geoenvironmental Engineering, **148**(6): 04022044. American Society of Civil Engineers.
- Zhao, R., Leung, A.K., and Knappett, J.A. 2022b. Thermally induced ratcheting of a thermo-active reinforced concrete pile in sand under sustained lateral load. Géotechnique,: 1–14. ICE Publishing. doi:10.1680/jgeot.21.00299.
- Zhao, S., Evans, T.M., Zhou, X., and Zhou, S. 2016. Discrete element method investigation on thermallyinduced shakedown of granular materials. Granular Matter, **19**(1). doi:10.1007/s10035-016-0690-5.
- Zhao, S., Zhao, J., and Lai, Y. 2020. Multiscale modeling of thermo-mechanical responses of granular materials: A hierarchical continuum–discrete coupling approach. Computer Methods in Applied Mechanics and Engineering, **367**: 113100. doi:10.1016/j.cma.2020.113100.
- Zhou, C., Ng, C.W.W., and Wang, S. 2017. Modelling volume changes of sand under thermal loads: a preliminary attempt. Géotechnique Letters, **7**(1): 68–72.
- Zoback, M.D. 2010. Reservoir geomechanics. Cambridge University Press.

572

573

587	Notations	
588	A_0	'intrinsic' dilatancy parameter
589	b^M	yield-to-memory surface distance
590	$ ilde{b}_b^M$	relative position of the memory and the dilatancy surfaces
591	b_{ref}	reference distance for normalization
592	b_0	hardening factor
593	С	compression-to-extension strength ratio
594	c_h	hardening parameter
595	C_u	coefficient of uniformity
596	d	particle size
597	D	dilatancy coefficient
598	D_R	relative density
599	D_{R0}	initial relative density
600	d_{50}	mean particle size
601	e	void ratio
602	\boldsymbol{e}	deviatoric strain tensor
603	e_c	void ratio at critical state
604	e_0	initial void ratio
605	e_r	reference critical void ratio, originally e_0 in Liu et al. (2019)
606	e_T	terminal void ratio
607	e_{max}	maximum void ratio
608	e_{min}	minimum void ratio
609	f	yield surface
610	f^B	bounding surface
611	f^D	dilatancy surface
612	f^{M}	memory surface
613	f_{shr}	memory surface shrinkage geometrical factor
614	g	interpolation function in triaxial space ($g = 1$ when $\eta > \alpha$; $g = c$ when $\eta < \alpha$)
615	$g(\theta)$	interpolation function for Lode angle dependence
616	G	shear modulus
617	G_0	dimensionless shear modulus
618	h	hardening factor

619	h^M	memory-counterpart of the hardening coefficient
620	h_0	hardening parameter
621	L	plastic multiplier
622	L^{M}	memory-counterpart of the plastic multiplier
623	m	yield locus opening parameter
624	m^M	memory locus opening parameter
625	M^d	stress ratio of dilatancy surface in triaxial space
626	M^b	stress ratio of bounding surface in triaxial space
627	M_c^b	stress ratio of bounding surface associated with compression in triaxial space
628	M	stress ratio of critical surface in triaxial space
629	\widetilde{M}^d	opposite projection stress ratio on the dilatancy surface in triaxial space
630	\widetilde{M}^M	opposite projection stress ratio on the memory surface in triaxial space
631	N	number of loading cycles
632	n	pre-set material parameter ($n = 0.5$)
633	n	unit tensor normal to the yield locus
634	$n^{b,d}$	void ratio dependence parameters
635	p_{atm}	atmospheric pressure
636	p	mean stress
637	p'	effective mean stress
638	p_0'	initial effective mean stress
639	q	deviatoric stress
640	R'	deviatoric plastic flow direction tensor
641	r	deviatoric stress ratio tensor
642	$ ilde{m{r}}$	projection of $m{r}$ on the yield surface along $-m{n}$
643	$ ilde{m{r}}^d_{ heta}$	projection of \boldsymbol{r} on the dilatancy surface along $-\boldsymbol{n}$
644	r_{in}	initial load-reversal tensor
645	r^M	image deviatoric stress ratio point on the memory locus
646	$ ilde{m{r}}_{ heta}^{M}$	projection of \boldsymbol{r} on the memory surface along $-\boldsymbol{n}$
647	$oldsymbol{r}_{ heta}^{b,c,d}$	bounding, critical and dilatancy deviatoric stress ratio tensor
648	$oldsymbol{r}_{ heta+\pi}^b$	projection onto the bounding surface with relative Lode angle $\theta + \pi$
649	S	auxiliary parameter ($s = 1$ when $\eta > \alpha$; $s = -1$ when $\eta < \alpha$)
650	s	deviatoric stress tensor

651	T	temperature
652	w	pre-set material parameter ($w = 2$)
653	<i>x</i> _{1,2,3}	line-segments defined to derive memory surface contraction law
654	ΔT	temperature variation
655	ΔD_{RT}	maximum change in relative density
656	α	back-stress ratio tensor
657	$oldsymbol{lpha}^M$	memory back-stress ratio tensor
658	eta_0	dilatancy memory parameter, originally β in Liu et al. (2019)
659	σ_z	vertical stress
660	η	stress ratio in triaxial space
661	η_{in}	initial load-reversal stress ratio
662	ε_a	axial strain of sand
663	$arepsilon^e$	elastic strain of sand
664	$arepsilon^p$	plastic strain of sand
665	\mathcal{E}_{v}	volumetric strain of sand
666	$arepsilon_r$	radial strain of sand
667	$arepsilon_{th}$	thermal strain of sand
668	β	volumetric thermal expansion coefficient of the solid grains
669	ζ	memory surface shrinkage parameter
670	θ	relative Lode angle
671	λ_c	shape parameter of critical state line
672	μ_0	ratcheting parameter
673	υ	Poisson's ratio
674	ξ	shape parameter of critical state line
675	ψ	state parameter
676		